Journal of Materials Chemistry B

PAPER

View Article Online
View Journal | View Issue

Cite this: J. Mater. Chem. B, 2014, 2, 2714

Bifunctional pH-sensitive Zn(II)–curcumin nanoparticles/siRNA effectively inhibit growth of human bladder cancer cells *in vitro* and *in vivo*†

Zhou-Hao Xing,‡[a] Jin-Huan Wei,‡[b] Tuck-Yun Cheang,‡[c] Zong-Ren Wang,‡[b] Xiao Zhou,[a] Sha-Sha Wang,[a] Wei Chen,[b] Shen-Ming Wang,[c] Jun-Hang Luo*[b] and An-Wu Xu*[a]

Received 18th November 2013
Accepted 18th February 2014

DOI: 10.1039/c3tb21625j

www.rsc.org/MaterialsB

To overcome drug resistance, the combination of two or more therapeutic strategies with different mechanisms has received much attention in recent years. In this study, a common approach has been used to process curcumin and Zn^{2+} into colloidal dispersions known as "nanoparticles", which are cheap and easy to prepare with high reproducibility. This novel vehicle has good biocompatibility and high cellular uptake for simultaneously delivering the curcumin drug and siRNA into tumor cells. Complexation of Zn^{2+} with curcumin enhances the aqueous solubility of the hydrophobic drug curcumin and further improves the cellular uptake and bioavailability. The acid-labile coordination Zn(II)–O bond in Zn(II)–curcumin drug nanoparticles (Zn(II)–Cur NPs) can respond to tumor intracellular acidic pH environments to release curcumin, and promoting acid-triggered intracellular drug release. The positively charged Zn(II)–Cur NPs can efficiently deliver siRNA into human bladder cancer cells, protect siRNA against enzymatic degradation, and facilitate the escape of loaded siRNA from the endosome into the cytoplasm, which successfully downregulates the targeted EIF5A2 oncogene and consequently inhibits cancer cell growth *in vitro* and *in vivo*. Proliferation and migration of cancer cells are inhibited by silencing the expression of EIF5A2 and increasing the ratio of pro-apoptotic BAX to anti-apoptotic BCL-2. *In vitro* and *in vivo* experiments have demonstrated that bifunctional Zn(II)–Cur NPs/siEIF5A2 can combine chemotherapy with gene therapy to afford higher therapeutic efficacy than the individual therapeutic protocols.

Introduction

To overcome drug resistance, the combination of two or more therapeutic strategies with different mechanisms has received much attention in recent years.[1] Small interfering RNA (siRNA) has shown great potential for the treatment of diseases, such as cancer, inflammation, diabetes, and neurodegenerative diseases.[2] Therefore, the combination of traditional chemotherapy with newly emerging siRNA-based gene therapy will enhance the therapeutic efficacy over the two independent treatments.[1c,3] The major challenge hindering the potential of siRNA resides in the lack of safe and effective delivery vehicles.[4] Both viral and non-viral vectors have been investigated in this area. Non-viral gene delivery systems are safer and easier to manufacture than viral vectors. However non-viral vectors developed so far have shown low transfection efficiency as compared to viral vectors.[5]

Recent studies have demonstrated that curcumin (1,7-bis-[4-hydroxy-3-methoxyphenyl]-1,6-heptadiene-3,5-dione, Scheme 1) and related β-diketone derivatives are potent modulators of arachidonic acid metabolism.[6] As a natural antitumor drug, curcumin is the principal curcuminoid of the popular Indian spice turmeric, a member of the ginger family (Zingiberaceae).[7] It has been reported that curcumin shows good anti-tumor activity, because curcumin can influence the release of arachidonic acid and its metabolites by inhibiting the phosphorylation of cytosolic phospholipase A2, expression of cyclooxygenase and the enzyme activity of lipoxygenase for killing the cancer cells.[8] Additionally, curcumin can induce an increase in the ratio of pro-apoptotic BAX to anti-apoptotic BCL-2 to inhibit proliferation and migration of cancer cells.[9] However, poor aqueous solubility of curcumin is generally related to low cellular uptake and bioavailability, how to increase the half-life *in vivo* of the poorly water-soluble curcumin

[a]Division of Nanomaterials and Chemistry, Hefei National Laboratory for Physical Sciences at Microscale, University of Science and Technology of China, Hefei, 230026, China. E-mail: anwuxu@ustc.edu.cn

[b]Department of Urology, First Affiliated Hospital, Sun Yat-Sen University, Guangzhou, 510080, China. E-mail: luojunh@mail.sysu.edu.cn

[c]Department of Vascular Surgery, First Affiliated Hospital, Sun Yat-Sen University, Guangzhou, 510080, China

† Electronic supplementary information (ESI) available: EDS spectrum, SEM and TEM images, zeta potential, drug release profiles, toxicity and changes of body weight. See DOI: 10.1039/c3tb21625j

‡ These authors contributed equally to this work.

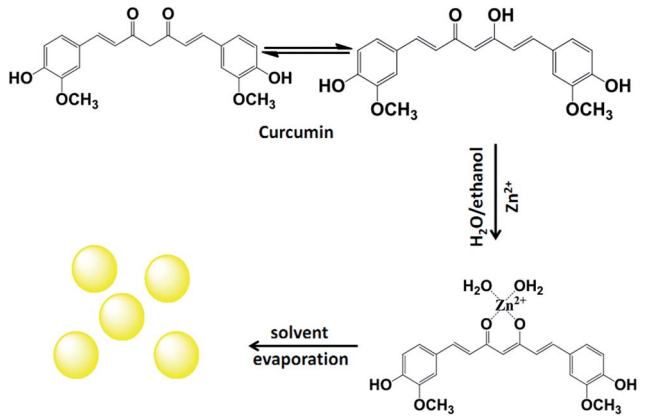

Scheme 1 Chemical structure of curcumin molecules and schematic illustration of the Zn(II)–curcumin nanoparticle formation.

drug remains a major challenge during drug formulations.[10] Previous studies showed that the 1,3-diketone part of curcumin can transform automatically into a keto–enol tautomeric form; the keto–enol form is more stable and can easily chelate the metal ions, such as Zn^{2+} and Cu^{2+}.[11] It should be noted that complexation of curcumin with metal ions will strongly increase the aqueous solubility of hydrophobic curcumin, which is beneficial for cellular uptake and bioavailability.

Most of the non-viral vehicles such as Au nanoparticles (NPs),[12] carbon nanotubes,[13] and silica[14] are not biodegradable; degradation of some biodegradable polymers, for example PLGA,[15] induces acidic oligomers and leads to a low pH that is harmful to cells.[3a] To avoid unnecessary molecular species from nanovectors entering the cells and achieve with the fewest side effects, herein, we use the hydrophobic curcumin natural drug itself to directly fabricate a nanosized hydrophilic carrier (Zn(II)–curcumin NPs) with high gene transfection efficacy for Human Bladder Cancer (HBC) cells *in vitro* and *in vivo*. As is well known, the pH around cancerous tissues is more acidic (pH 4–6) compared to the blood and normal tissues, which allows for the controlled drug release from the pH-sensitive delivery nanovectors that could respond to acidic environments. Since curcumin is conjugated to Zn^{2+} by an acid-labile coordinate bond, Zn(II)–Cur NPs should display intracellular pH-sensitive curcumin release to cancer cells. It has been reported that the overexpression of EIF5A2 is an independent predictor of the outcome in patients of human bladder cancer;[16] we use siEIF5A2 as targeted siRNA in our experiments. The obtained bifunctional Zn(II)–curcumin nanoparticles (Zn(II)–Cur NPs) loaded with siRNA have shown tumor acidity-targeted drug and siRNA delivery, few side effects, and high antitumor efficacy based on the combination of chemotherapy and gene therapy.

Experimental section

Cell culture and reagents

The curcumin and $Zn(NO_3)_2$ were purchased from Aladdin (Shanghai, China, www.aladdin-reagent.com). The human bladder tumor cell lines HBC were obtained from the American Type Culture Collection. HBC cells were cultured in Dulbecco's modified Eagle's medium (DMEM; CellGro) with 10% fetal bovine serum (CellGro) at 37 °C and 5% CO_2. The siRNA targeting human EIF5A2 (siEIF5A2) and the negative control siRNA (siNC) not targeting any known mammalian mRNA were supplied by Shanghai GenePharma Co. Ltd. (Shanghai, China): the oligoribonucleotide sequence of short interference RNA to repress EIF5A2 is listed as follows: sense: 5′-UGGUGAA GUUCGUGAGGAUUU-3′; antisense: 5′-AUCCUCACGAACUU CACCAUU-3′.

Fluorescein-tagged siRNA (FAM-siRNA) was synthesized by modification of the 3′-end of the sense strand of the siEIF5A2 with fluorescein. Mouse anti-EIF5A2 and anti-GAPDH purchased from Abcam (Cambridge, UK) were used for western blotting and immunohistochemistry.

Synthesis of Zn(II)–curcumin coordination compound nanoparticles and characterization

In a typical synthetic route, $Zn(NO_3)_2$ (2 mL, 2 mM) aqueous solution and curcumin (2 mL, 2 mM in ethanol) solution were mixed in a 25 mL glass beaker with addition of 16 mL of double distilled water. The mixture was kept at 50 °C for 6 hours in a water bath. The yellow Zn(II)–Cur precipitates produced from solvent evaporation were collected by centrifugation and then washed with double distilled water several times. Finally, the products were dried at 40 °C under vacuum overnight.

The contact angle was measured on a contact angle meter SL200B (Kino Industry, USA) at room temperature. Water droplets (about 10.0 μL) were dropped carefully onto the tableted curcumin and Zn(II)–Cur NP surface. Scanning electron microscopic (SEM) images were taken with a JEOL JSM-6700F operated at 15 kV. Transmission electron microscopic (TEM) images and energy dispersive X-ray spectroscopy (EDS) spectrum were obtained on a JEOL-2010 microscope with an accelerating voltage of 200 kV. Fourier transform infrared (FTIR) spectra were recorded on a Nicolet Nexus spectrometer with samples embedded in KBr pellets.

In vitro drug release studies

In vitro drug release studies were performed for a period of 36 hours at two different pHs (7.4 and 5.0). 10 mg of Zn(II)–Cur NPs were added into 60 mL PBS (10 mM) and then the mixture was divided into 20 mL tubes (10 set each having 3 tubes). The tubes were then incubated in a water bath shaker at 37 °C.

At definite time, one set of tubes were taken out and centrifuged at 1200 rpm for 3 min, and the precipitate was collected because free curcumin is completely insoluble in water.[17] The precipitate was re-dissolved in 3 mL ethanol and the amount of drug released was quantified spectrophotometerically at a wavelength of 427 nm.

Gel electrophoresis

The Zn(II)–Cur NPs and siRNA were mixed at the mass ratios of 1 : 1, 10 : 1, 30 : 1, 50 : 1, and 100 : 1, respectively, forming different compositions of formulation. *In vitro* transfection was performed as we previously described.[18]

The resulting Zn(II)–Cur NP/siRNA complexes were allowed to stay at room temperature for 30 min for further complexation. The resulting complexes were centrifuged at 5000 rpm for 5 min, and then redispersed in 15 μL phosphate buffered saline (PBS, pH 7.4) solution. The samples were loaded onto 3% agarose gels pre-stained with ethidium bromide (EtBr, 0.1 μg mL^{-1}), electrophoresis was carried out at 15 mA for 1 hour, and the bands were visualized on a UV transilluminator.

HBC cells were seeded in 96-well plates at a density of 8×10^3 cells per well for MTT assay. And then the cells were transfected with different concentrations of Zn(II)–Cur NPs (50 μg mL^{-1}, 100 μg mL^{-1} and 150 μg mL^{-1}) carrying 50 nM siNC, or Lipofectamine 2000 conjugated same amount of siNC, or the siNC only, or PBS solution as control. The treated cells were cultured at 37 °C with 5% CO_2 for four days, the former medium was removed and replaced with 100 μL of fresh medium, then 20 μL of 5 mg mL^{-1} MTT was added to each well for 4 h, the medium was removed again and 150 μL of dimethyl sulphoxide (DMSO) was added. The plates were measured at a wavelength of 490 nm after shaking at 600 RPM for 10 min.

In vitro transfection and the distribution of Zn(II)–Cur NPs/FAM-siEIF5A2

In vitro transfection was performed as we previously described.[18] Briefly, HBC cells were seeded to three 24-well plates at a density of 5×10^4 cells per well and incubated overnight at 37 °C in 5% CO_2 to achieve 60–80% confluence. The cells were transfected with various predetermined formulations. After 6 h, cells were analyzed for FAM-siEIF5A2 uptake by inverted fluorescence microscopy (Olympus, IX71, Japan). Cells were then collected by trypsinization, centrifuged, (2000 × *g*, 3 min) and dispersed in PBS solution and analyzed by flow cytometry assay (Beckman Coulter).

For confocal laser scanning microscopy (CLSM) observations, HBC cells (5×10^4 cells per well) were seeded in a 35 mm glass bottom culture dish (MatTek Corporation) and incubated for 24 h at 37 °C in 5% CO_2. Then the former cell culture medium was replaced with 500 μL of serum-free DMEM containing different mass ratios of the Zn(II)–Cur NP/FAM-siEIF5A2 complex in each well. At predetermined time intervals, after removal of the medium, cells were washed several times with the PBS solution. The cell nuclei were then stained with DAPI (4′,6′-diamidino-2-phenylinodole, Sigma) for 5 min. The cells were stained with Lyso-tracker Red and directly observed by Olympus FluoView confocal microscopy and analyzed with FV10-ASW viewer software (Olympus, Tokyo, Japan).

Analysis of EIF5A2 expression

In brief, HBC cells (5×10^4) were seeded in three 24-well plates and incubated at 37 °C in 5% CO_2 for 24 h to reach about 70% confluence. Zn(II)–Cur NPs/siEIF5A2 (50 nM or 100 nM or 150 nM of siEIF5A2 respectively, at a mass ratio of 50 : 1), or unloaded Zn(II)–Cur NPs, or Zn(II)–Cur NPs/siNC (150 nM of siNC) or PBS solution only were added and incubated with the cells for 24 h (for mRNA isolation) or 48 h (for protein extraction).

The expression of EIF5A2 mRNA was analyzed by real time-PCR assay. Total RNA was extracted with TRIzol reagent (Invitrogen, Carlsbad, California, USA). The relative cDNA was synthesised with a PrimeScript RT reagent Kit (Promega, Madison, WI, USA). Real-time PCR was carried out using an ABI 7900HT fast real-time PCR system (Applied Biosystems, Foster City, California, USA). Amplification consisted of 30 cycles of 30 s at 94 °C, 30 s at 55 °C and 60 s at 72 °C. The qPCR primers for EIF5A2 and GAPDH are listed as follows: EIF5A2-specific primer:

F: 5′-GGACGACCATGCAAAATAGTGG-3′; R: 5′-TGCCCGTGAAAA TATCAATTCCA-3′.

GAPDH-specific primer: F: 5′-CCCACATGGCCTCCAAGGAGTA-3′; R: 5′-GTGTACATGGCAACTGTGAGGAGG-3′.

An equal amount of whole-cell lysate was resolved by sodium dodecylsulfate polyacrylamide gel electrophoresis and transferred onto a polyvinylidene difluoride membrane (Pall Corp., Port Washington, NY), followed by incubation with primary mouse monoclonal antibodies for Western blotting analysis. Primary and secondary antibodies were diluted using 5% milk in PBST, and incubation was performed at room temperature for 1 hour. The immune reactive proteins were analyzed by enhanced chemiluminescence detection reagents (Amersham Biosciences, Uppsala, Sweden) according to the manufacturer's instructions.

MTT assay, cell apoptosis analyses and cell cycle analyses post Zn(II)–Cur NPs/siEIF5A2 transfection

Cell proliferation after transfection with siEIF5A2 by Zn(II)–Cur NPs was determined with MTT assay. HBC cells were seeded in 96-well plates at a density of 8×10^3 cells per well. Different doses of siEIF5A2 loaded by Zn(II)–Cur NPs were prepared in 24-well plates for further use. 20 μL of MTT (Sigma-Aldrich) solution (5 mg mL^{-1}) was added into each well and incubated for 4 h after treatment with various formulations for 24, 48, 72, 96, 120, and 144 h. The reaction ended by drawing off all medium and adding 150 μL of DMSO. The optical density was determined on a microplate spectrophotometer at a wavelength of 490 nm. MTT was conducted to detect the human bladder cancer cell viability by treatment with different concentrations of $Zn(NO_3)_2$ (0, 50 nM, 100 nM, 150 nM, 200 nM) at different times (12 h, 24 h, 48 h). Each group involved 6 parallel experiments.

For apoptosis analysis, HBC cells were seeded in a 24-well plate at a density of 5×10^4 cells per well. HBC cells were stained with Annexin V-PE and propidium iodide (PI) 48 h after the transfection using an Annexin V apoptosis detection kit (BD Biosciences). As viable cells are both Annexin V-PE and PI negative, the percentage of apoptotic cells was quantified by flow cytometry.

For cell cycle analysis, HBC cells were seeded in a 24-well plate at a density of 5×10^4 cells per well. 48 h after transfected with Zn(II)–Cur NPs/siEIF5A2, or Zn(II)–Cur NPs/siNC, or unloaded Zn(II)–Cur NPs, or PBS solution only, each well was trypsinized and cells were fixed using 70% ethanol, followed by staining with a Coulter DNA-Prep Reagents kit (Beckman Coulter, Fullerton, CA). The cellular DNA content was

determined using flow cytometry (Becton Dickinson, San Jose, CA, USA) for each sample. All the experiments were performed in triplicate.

In vivo fluorescence imaging

For *in vivo* imaging, 400 mL of Zn(II)–Cur NPs/FAM-siEIF5A2, or an equal dose of free FAM-siEIF5A2, or PBS solution were injected in female mice bearing HBC tumors intratumorally. Animals were placed onto a warmed stage inside an IVIS light-tight chamber, and anesthesia was carried out with 2.5% isoflurane. Image acquisition was performed at different time intervals on a Xenogen IVIS Lumina system (Caliper Life Sciences, USA). Results were analyzed by Living Image 3.1 software (Caliper Life Sciences, USA).

Tumor suppression study *in vivo*

BALB/c nu/nu immune deficient mice (6 weeks old, 18–20 g) were purchased from Shanghai Slac Laboratory Animal Co., Ltd. (Shanghai, China). 4×10^7 HBC cells in 100 μL PBS solution were injected subcutaneously into the dorsal flanks of each mouse using a 25-gauge needle. When the HBC cells developed a tumor (tumor volume about 100 mm^3), the mice were randomized into four treatment groups, with six mice in each group, respectively, Zn(II)–Cur NPs/siEIF5A2 (20 μg of siEIF5A2 per injection, 50 : 1 mass ratio), or an equal amount of unloaded Zn(II)–Cur NPs, or siEIF5A2 only, or PBS solution were injected directly into tumors. The treatments were repeated every week for total five times. The long and short axial lengths of the tumors were measured every other day. To clarify the side-effect of the Zn(II)–Cur NP/siEIF5A2 complex, 20 C57BL mice were divided to four groups with injection of PBS, Zn(II)–Cur NPs, Zn(II)–Cur NPs/siNC and Zn(II)–Cur NPs/siEIF5A2, respectively. We injected two times total in fourteen days, and the body weight of mice was recorded every two days. The dose of Zn(II)–Cur NPs by tail vein injection was 50 mg kg^{-1}, which is the same as intratumoral injection. The Institute Research Medical Ethics Committee of Sun Yat-Sen University granted approval for this study.

Statistical analysis

All experiments were repeated three times at least. Data were presented as means ± standard deviation. Statistical significance ($P < 0.05$) was evaluated by using Student's *t*-test when only two groups were compared. Evaluation of significance was performed using one-way analysis of variance (ANOVA) followed by Bonferroni's *post-hoc* test if more than two groups were compared. In all tests, the statistical significance was set at $P < 0.05$.

Results and discussion

Synthesis and characterization

The 1,3-diketone moiety of the curcumin ligand (L) can transform automatically to a more stable keto–enol tautomeric form with more strongly delocalized unpaired electrons, easily chelating the Zn^{2+} metal ion (M) to form a ML type complex (Scheme 1).[11] Zn(II)–curcumin nanoparticles (Zn(II)–Cur NPs) were prepared by a solvent evaporation method using H_2O and ethanol (with a volume ratio H_2O–ethanol = 9 : 1) as mixed solvent. The quick evaporation rate at 50 °C led to the depletion of ethanol, and yellow Zn(II)–Cur NPs precipitated from solution (see the Experimental section).

The obtained Zn(II)–Cur NPs were characterized by scanning electron microscopy (SEM) and transmission electron microscopy (TEM) measurements (Fig. 1). A typical SEM image of the obtained Zn(II)–Cur NPs indicates that the sample consists of a large number of spherical nanoparticles with a diameter of about 80–500 nm (Fig. 1A). From the TEM image (Fig. 1B) it can be seen that each nanosphere has a rough surface, which is beneficial for siRNA attachment. Energy dispersive spectrum (EDS) analysis shows that the molar ratio of Zn(II) to curcumin in Zn(II)–Cur NPs is *ca.* 2.1/97.9 (Fig. S1†).

A contact angle meter was used to investigate the wetting behavior of water droplets (10 μL) on the surface of tableted curcumin and Zn(II)–Cur NPs for determining hydrophobicity/hydrophilicity. From Fig. 2, it can be clearly seen that curcumin is hydrophobic and poorly water-soluble, when curcumin was coordinated with Zn^{2+} to form Zn(II)–Cur NPs, the interaction of Zn(II)–water molecules (Scheme 1) leads to the addition of hydrogen bond with H_2O molecules making the surface hydrophilic.[19] The contact area between the droplet and the underlying surfaces of Zn(II)–Cur NPs is much larger than that of curcumin, indicating good aqueous solubility of Zn(II)–Cur NPs. Enhancement of aqueous solubility is beneficial to

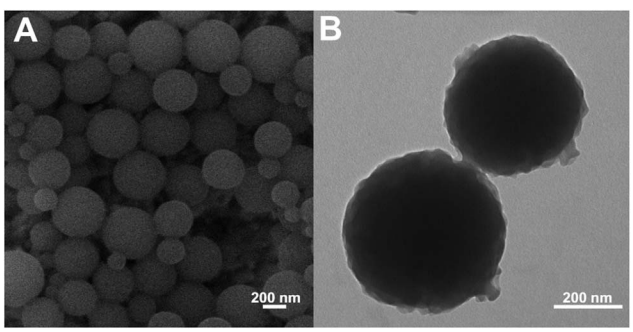

Fig. 1 (A) SEM image of Zn(II)–Cur NPs and (B) TEM image of Zn(II)–Cur NPs.

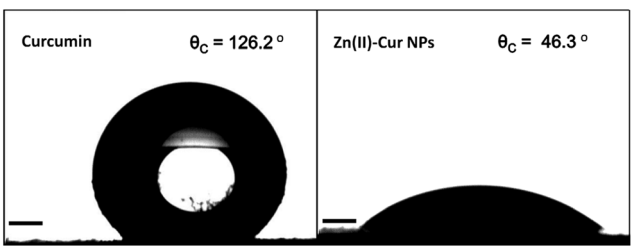

Fig. 2 Images of a water droplet sitting on the tableted surfaces of curcumin with a contact angle of 126.2 ± 2.46° (left), and Zn(II)–Cur NPs with a contact angle of 46.3 ± 1.02° (right). Scale bar: 0.5 mm.

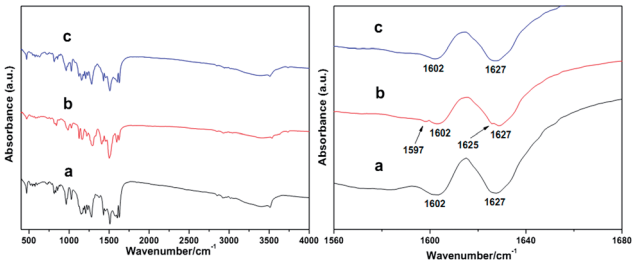

Fig. 3 (Left) IR spectra of curcumin (a), Zn(II)–Cur NPs (b) and precipitates (c) formed from Zn(II)–Cur NP PBS solution by adjusting the pH to 5; (right) the inserted illustrations are expanded IR spectra in the range from 1590 to 1680 cm^{-1}.

improve the cellular uptake and bioavailability of the hydrophobic drug curcumin.[10b]

IR spectra of curcumin (Fig. 3a) show that the 1627 and 1602 cm^{-1} bands are attributed to the mixtures of stretching vibrations of (C=C) and (C=O) in curcumin,[20] and these two bands are red-shifted to a small extent to 1625 and 1597 cm^{-1} in the Zn(II)–Cur NPs demonstrating the formation of the Zn(II)–O band in Zn(II)–Cur NPs (Fig. 3b).[11] The 1627 and 1602 cm^{-1} bands remain strong because the molar ratio of Zn(II) to curcumin in Zn(II)–Cur NPs is very low (about 2.1/97.9).

Since Zn^{2+} is complexed to curcumin by an acid-labile coordination Zn(II)–O bond, the Zn(II)–Cur NPs were treated with phosphate buffered saline (PBS) solution at pH = 5 for 4 h and the yellow precipitates from the colourless and transparent solution were analyzed by IR spectra. As shown in Fig. 3c, the peaks appeared at 1627 and 1602 cm^{-1} correspond to that of curcumin, indicating pH-sensitive curcumin release from Zn(II)–Cur NPs. It is known that the pH-dependent drug-loading and releasing properties are favorable for cancer therapy owing to the microenvironments of extracellular tumor tissues and intracellular lysosomes and endosomes are acidic (pH = 4–6),[21] facilitating active drug release from the Zn(II)–Cur NP-based curcumin delivery vehicles.[22] Fig. S2† shows the pH-dependent release profiles of curcumin from the Zn(II)–Cur NPs at pH = 5 and pH = 7.4. At pH = 5, about 90% of curcumin was released into the solution within 12 h, but at pH 7.4, only about 18% was released within 12 h, thus demonstrating this complex carrier to be pH sensitive.

siRNA-binding efficiency

A gel electrophoresis shift assay was performed to confirm complexation of Zn(II)–Cur NPs and siRNA. From the result of agarose gel electrophoresis (Fig. 4) by checking the intensities of the bands, it can be seen that when Zn(II)–Cur NPs were mixed with siRNA at a mass ratio of 50 : 1 and higher, siRNA is completely formed into the complex with Zn(II)–Cur NPs. These results suggest that the optimal mass ratio between Zn(II)–Cur NPs and siRNA is 50 : 1, which is used in the following experiments. ζ-Potential measurements demonstrate that the obtained Zn(II)–Cur NPs bear a positive surface potential with +22.3 mV, which leads to an electrostatic interaction with the negatively charged siRNA to form the Zn(II)–Cur NP/siRNA

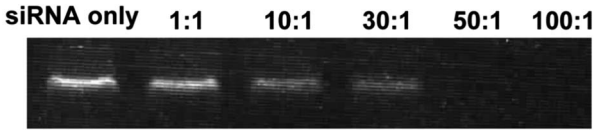

Fig. 4 Binding ability of Zn(II)–Cur NPs to siRNA at different mass ratios demonstrated by the gel electrophoresis assay.

complex (Fig. S3†). The SEM and TEM images of Zn(II)–Cur NP/siEIF5A2 complexes at a mass ratio of 50 : 1 were obtained, as displayed in Fig. S4.† No obvious aggregation was observed. Moreover, the positively charged Zn(II)–Cur NPs/siEIF5A2 at a mass ratio of 50 : 1 (+15.4 mV, Fig. S5†) result in strong interactions with the negatively charged cell membranes, thus promoting highly efficient cellular uptake *in vitro* and in *vivo*.[23]

Transfection efficiency

Over expression of EIF5A2 is an independent predictor of outcome in patients with human bladder cancer (HBC),[16] so siEIF5A2 was used as targeted siRNA in following experiments. The efficiency of siRNA entering cancer cells was monitored by inverted fluorescence microscopy, the siEIF5A2 was labeled with fluorescein, and then the cellular uptake of the Zn(II)–Cur NP/FAM-siEIF5A2 complex in HBC cells was analyzed under an inverted fluorescence microscope. As shown in Fig. 5A, FAM-siEIF5A2 is clearly observed within the HBC cells after 6 h of incubation, indicating the internalization of Zn(II)–Cur NPs/siEIF5A2.

To further understand how the Zn(II)–Cur NP/FAM-siEIF5A2 complex affects the cell internalization of siRNA, HBC cells were incubated with the complex for 6 h; after quenching the

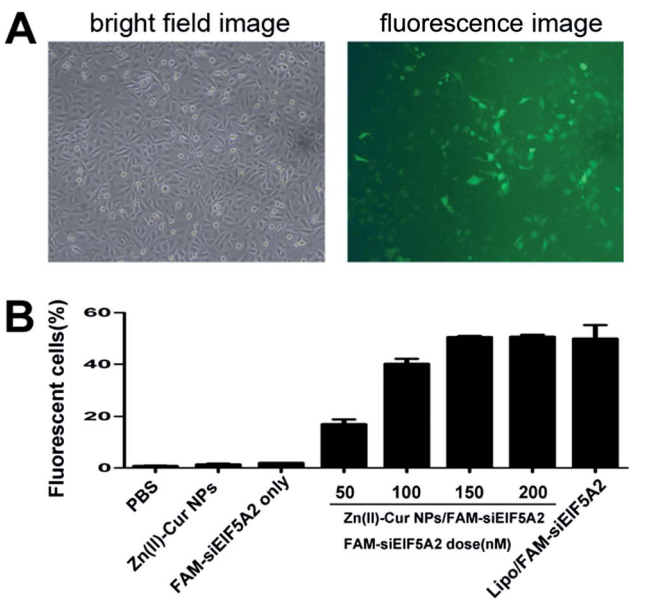

Fig. 5 (A) Inverted fluorescence microscopy images showing FAM-siEIF5A2 fluorescence after the final 6 h transfection. (B) Histograms and the mean ± SD of percentage of fluorescent cells detected by flow cytometry. The mean ± SD are cumulative results from three independent experiments.

extracellular fluorescence with trypan blue, the cells were subsequently analyzed by flow cytometry. As shown in Fig. 5B, for the Zn(II)–Cur NP/FAM-siEIF5A2 complex, the percentage of fluorescent cells increases with an increase in the dose of FAM-siEIF5A2. Obviously, when the FAM-siEIF5A2 dose is 150 nM, cells incubated with the Zn(II)–Cur NP/FAM-siEIF5A2 complex exhibit almost equal transfection efficiency as compared to the Lipofectamine 2000/FAM-siEIF5A2 complex. Transfection efficiency is not significantly enhanced when the dose of siEIF5A2 is increased to 200 nM. Thus, the optimal dose of siEIF5A2 delivery by Zn(II)–Cur NP transfection in HBC cells is 150 nM. From Fig. 5B, it can be clearly seen that Zn(II)–Cur NPs show high gene transfection efficacy with 50.76 ± 1.30%, which is as effective as commercial Lipofectamine 2000 for siEIF5A2 (150 nM) transfection (50.03 ± 8.94%). The high delivery efficiency suggests that the natural biodegradable anticancer drug curcumin based NPs can serve as promising novel vectors for siRNA delivery.

Intracellular distribution of FAM-labeled siEIF5A2

HBC cells were treated with Zn(II)–Cur NPs/FAM-siEIF5A2 to investigate whether siEIF5A2 loaded on Zn(II)–Cur NPs could escape from the lysosome, and the localization of NPs in cells was measured by CLSM. The cell nuclei were counterstained with DAPI. As shown in Fig. 6, the therapeutic effects of Zn(II)–Cur NPs were first investigated by the uptake behavior in HBC cells. FAM-siEIF5A2 strong fluorescence was distributed in the HBC cell cytoplasm and periphery of nuclei, suggesting efficient delivery of siRNA into cytoplasm due to the positively charged Zn(II)–Cur NPs. The cells were then labeled with Lyso-Tracker Red to visualize the late endosomes and lysosomes. The results reveal that although some FAM-siRNA was colocalized with lysosomes, there is a large amount of FAM-siEIF5A2 distributed throughout the cytoplasm, indicating that the Zn(II)–Cur NPs delivered siEIF5A2 successfully avoided the acidic lysosomes (Fig. 6). At endosomal pH (pH 5.0), Zn^{2+} ions can be released from the pH-sensitive Zn(II)–Cur NP/siEIF5A2 complex. Zn^{2+} ions may induce endosome membrane destabilization for the escape of siRNA.[24]

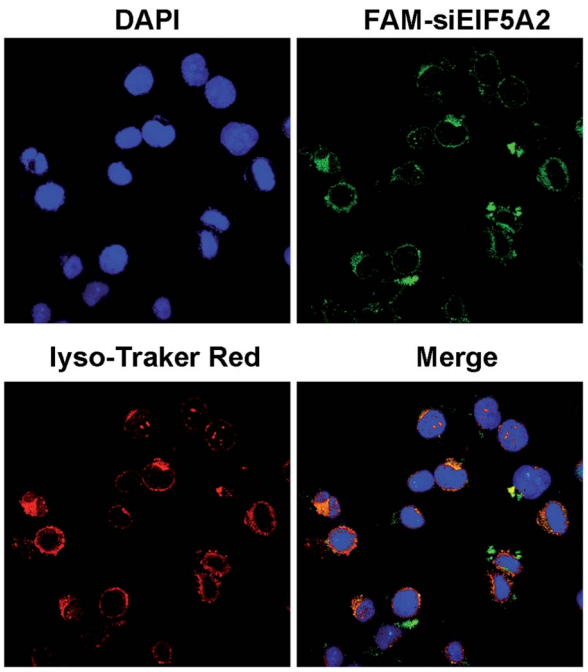

Fig. 6 Confocal laser scanning microscopy (CLSM) images of DAPI, FAM-siEIF5A2, Lyso-Traker Red and Merge in HBC cells after treated with Zn(II)–Cur NPs/FAM-siEIF5A2 and dyes for 6 h.

Cell proliferation, cell cycle analyses, and apoptosis after EIF5A2 knockdown

EIF5A2 messenger RNA (mRNA) and protein expression levels were analyzed by RT-PCR and western blotting, respectively, to confirm the knockdown of EIF5A2 in HBC cells after siEIF5A2 packaged Zn(II)–Cur NP transfection. As shown in Fig. 7A, the EIF5A2 mRNA levels were decreased in a siEIF5A2 dose-dependent manner, which were not observed in the Zn(II)–Cur NP/siNC complex group as compared to the control. Consistently, the levels of EIF5A2 protein changed in a similar dose-dependent manner (Fig. 7A). In general, these results indicate that Zn(II)–Cur NP/siEIF5A2 complex transfection can efficiently knockdown EIF5A2 at mRNA and protein levels in HBC cells.

Next, MTT assay was employed to evaluate the proliferation of HBC cells after Zn(II)–Cur NP/siEIF5A2 complex mediated EIF5A2 silencing. In Fig. 7B, as compared to the control, the Zn(II)–Cur NP/siEIF5A2 complex significantly reduced tumor cell proliferation in a siEIF5A2 dose dependent manner (150 nM, 28.87 ± 10.81%), and lower reduction was observed with the Zn(II)–Cur NPs (79.54 ± 5.09%). These results suggest that Zn(II)–Cur NP/siEIF5A2 complexes and Zn(II)–Cur NPs can largely reduce HBC cell proliferation *in vitro*. The Zn^{2+} concentration in the medium used in our experiment was about 2.87 μM. It can be clearly seen from Fig. S6† that no significant change in cell viability was found until the concentration of Zn^{2+} reached 200 μM in human bladder cancer T24 cells. So the toxicity of Zn^{2+} induced by Zn(II)–Cur NPs can be ignored at the concentration of 2.87 μM.

We also analyzed the cell cycle of HBC cells treated with various formulations using a Coulter DNA-Prep Reagents kit. The cellular DNA content from each sample was determined by flow cytometry. As shown in Fig. 7C, the Zn(II)–Cur NP/siEIF5A2 treated sample exhibits that the number of S phase cells decreases to 12.8% as compared with control groups. The results have proven that Zn(II)–Cur NP/siEIF5A2 treatment has highly efficient anti-tumor effects by cell cycle arrest *in vitro*.

It is found that a higher dose of siEIF5A2 results in more apoptotic cells, as clearly seen from Fig. 7D. Incubation with Zn(II)–Cur NPs/siEIF5A2 (150 nM siEIF5A2) at a mass ratio of 50 : 1 induced apoptosis in 31.5% of HBC cells, while incubation with Zn(II)–Cur NPs/siEIF5A2 (50 nM siEIF5A2) induced apoptosis in only 10.9% of HBC cells. Moreover, Zn(II)–Cur NPs and Zn(II)–Cur NPs/siNC (150 nM siNC) did not generate significant apoptosis (only 7.1% and 7.7%, respectively), clearly demonstrating that apoptosis is mainly attributed to siEIF5A2 down-regulation.

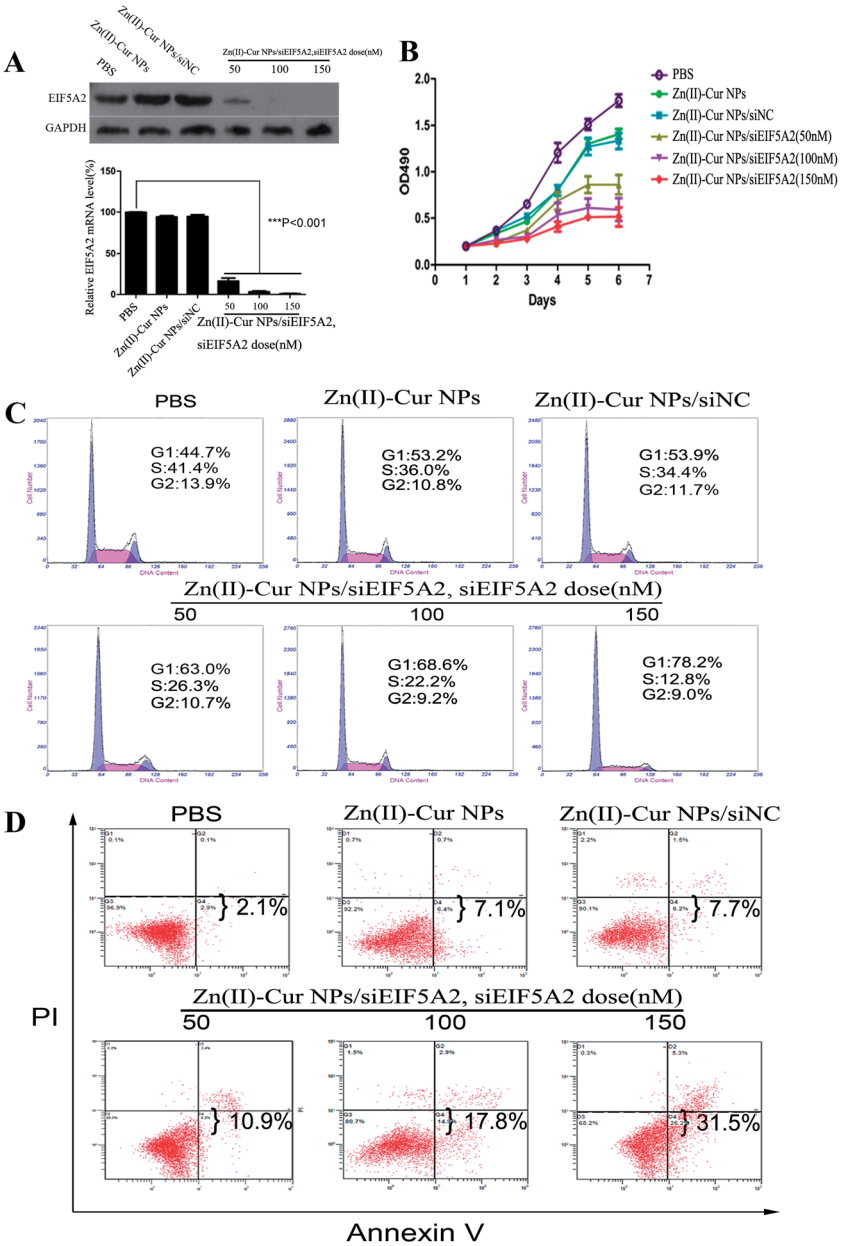

Fig. 7 The effect of EIF5A2 silencing mediated by Zn(II)–Cur NP transfection in HBC cells *in vitro*. (A) AKT1 expression and protein level after Zn(II)–Cur NP/siEIF5A2 transfection assessed by real time-PCR and western blotting, respectively. (B) MTT assay was conducted to evaluate the HBC cell viability after transfection of the Zn(II)–Cur NP/siEIF5A2 complex at different doses (*$P < 0.05$, treatment *vs.* control). (C) Cell cycle was determined by FACS analysis of Zn(II)–Cur NP mediated EIF5A2 knockdown in HBC cells for 48 h (1 of 3 replicates is shown). (D) Zn(II)–Cur NP/siEIF5A2 complex and other formulation treated HBC cells were stained with Annexin V-PE and PI, and analysis of apoptosis with flow cytometry.

Collectively, the above results have confirmed that Zn(II)–Cur NP/siEIF5A2 treatment has high anti-tumor effects, as evidenced by inhibition of proliferation, induction of apoptosis, and cell cycle arrest *in vitro*. The efficacious therapy may result from the enhanced intracellular uptake, the pH-sensitive delivery and the extracellular protection of curcumin and siRNA by Zn(II)–Cur nanocarriers. It is noted that curcumin itself also shows good anti-tumor activity, because curcumin can affect the release of arachidonic acid and its metabolites by inhibiting the phosphorylation of cytosolic phospholipase A2, expression of cyclooxygenase and the enzyme activity of lipoxygenase to kill the cancer cells.[8] Our *in vitro* experiments have clearly revealed that the combination of curcumin chemotherapy and gene therapy leads to higher effects than individual therapeutic protocols.

FAM-siEIF5A2 biodistribution in tumor tissues and tumor suppression study

Zn(II)–Cur NPs/FAM-siEIF5A2 were intratumorally injected into the subcutaneous xenograft of mice, and the distribution of FAM-siEIF5A2 in tumor tissues was assessed by *in vivo* imaging

technology. Naked FAM-siEIF5A2 and phosphate-buffered saline were used as controls. After the injection for 0.5 h, Zn(II)–Cur NPs/FAM-siEIF5A2 exhibit stronger fluorescence intensity as well as a larger fluorescence distribution area at the tumor tissue than naked FAM-siEIF5A2 (Fig. 8A). Zn(II)–Cur NPs carrying FAM-siEIF5A2 reveal excellent tissue penetrability to the tumor sites and subsequent distribution in a larger tumor area compared to naked FAM-siEIF5A2. The Zn(II)–Cur NP/siEIF5A2 group continuously displays strong fluorescence at the tumor site for 16 h after injection, however, neither the naked FAM-siEIF5A2 nor the PBS treated group exhibits visible fluorescence after 8 h, therefore, it is suggested that the complexation between Zn(II)–Cur NPs and FAM-siEIF5A2 prevents nonspecific protein adsorption and aggregation of the NPs in tumor tissues.

Tumor frozen slices at 16 h post injection were stained with DAPI in order to get the distribution information in the central part of tumor, followed by CLSM observations for both FAM-siEIF5A2 and DAPI. DAPI staining was performed to locate the cancer cells. As shown in Fig. 8B, a significant amount of FAM-siEIF5A2 delivered from Zn(II)–Cur NP/FAM-siEIF5A2 complexes gradually passed through the cytomembrane and assembled in cytoplasm owing to the positively charged Zn(II)–Cur NPs. This phenomenon is likely due to protection of siRNA against nuclease degradation by positively charged Zn(II)–Cur NPs in tumor tissues.[25]

Antitumor growth effect of Zn(II)–Cur NPs/siEIF5A2 and expression levels of EIF5A2 and BCL-2 in tumor tissues

We examined the antitumor growth effect of Zn(II)–Cur NPs/siEIF5A2 by comparison with Zn(II)–Cur NPs and Zn(II)–Cur NPs/siNC *in vivo*. Athymic mice bearing HBC cell xenografts each received a weekly intratumoral injection of Zn(II)–Cur NPs/siEIF5A2 at a siRNA dose of 20 μg per injection for 5 times in total (Fig. 9A). Significant inhibition of tumor growth is markedly observed for 44 days after intratumoral injection of Zn(II)–Cur NPs/siEIF5A2, as clearly shown in Fig. 9B. The Zn(II)–Cur NP/siEIF5A2 group shows a tumor volume reduction of 75.92 ± 2.60% (Fig. 9C) and a tumor weight reduction of 88.35 ± 7.27% (Fig. 9D), respectively ($n = 6$ mice in the Zn(II)–Cur NP/siEIF5A2 treatment group; $^{***}P < 0.001$ *vs.* PBS treatment control mice). In a low dose of Zn(II)–Cur NP treatment groups, mice were exposed weekly for 44 days by injection to 1 mg/19 g body weight of Zn(II)–Cur NPs, which also slows down tumor growth (28.84 ± 6.82% v/v and 40.20 ± 11.59 wt% of volume/weight reduction; Zn(II)–Cur NPs group *vs.* PBS control group), in agreement with the results of MTT assay (Fig. 7B). This result indicates that cellular uptake and bioavailability of curcumin is strongly enhanced upon binding to Zn^{2+}, as compared to previous study achieving a similar therapeutic effect by oral gavage to 1 mg g^{-1} body weight of curcumin with a high dose.[26] The drug administrated in a low dose in our case could avoid detrimental side effects or undesirable immunological response. It is worth noting that as naked siRNA results in weak inhibition to tumor growth,[18b] therefore, it can be seen that combination of the two therapeutic strategies with different mechanisms can more efficiently prohibit cancer development as one plus one equals more than two.[1a–g]

Curcumin inhibits proliferation and migration by increasing the ratio of pro-apoptotic BAX to anti-apoptotic BCL-2 in cancer cells.[9] To further explore the mechanism underlying the antitumor growth effect mediated by combination of curcumin and siEIF5A2, the signaling pathways of EIF5A2 and BAX/BCL-2 regulating HBC cell growth were investigated. We analyzed the subcutaneous tumor tissues by western blotting after the

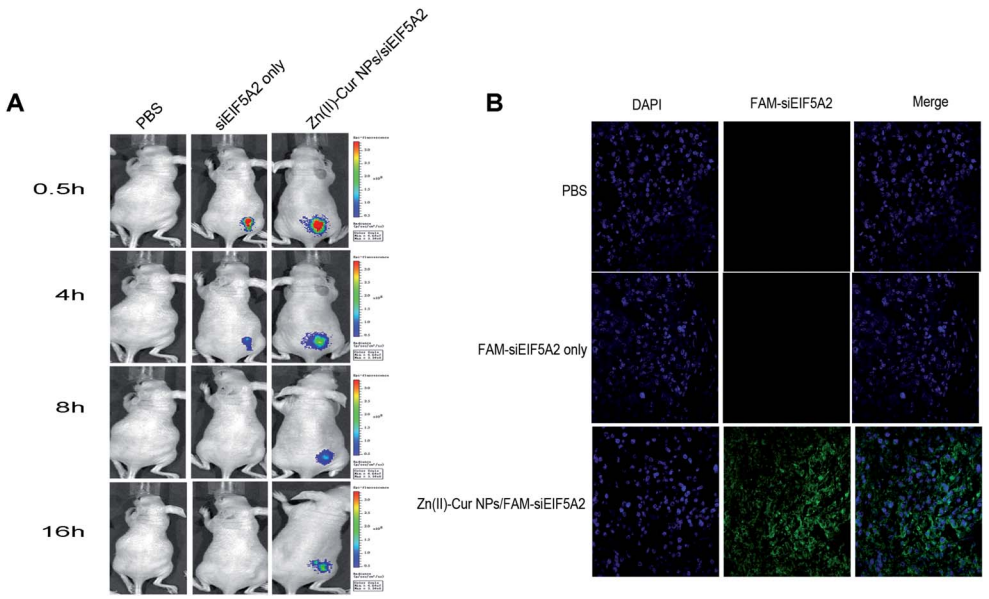

Fig. 8 (A) Fluorescence images of HBC cells xenograft-bearing mice after intratumoral injection of Zn(II)–Cur NPs/FAM-siEIF5A2, free FAM-siEIF5A2 or phosphate-buffered saline. (B) CLSM images show the distribution of FAM-siRNA in tumor following intratumoral injection of PBS, FAM-siRNA or Zn(II)–Cur NPs/FAM-siEIF5A2 (400×). siRNA was labeled with fluorescein (green) and cell nuclei were stained with DAPI (blue).

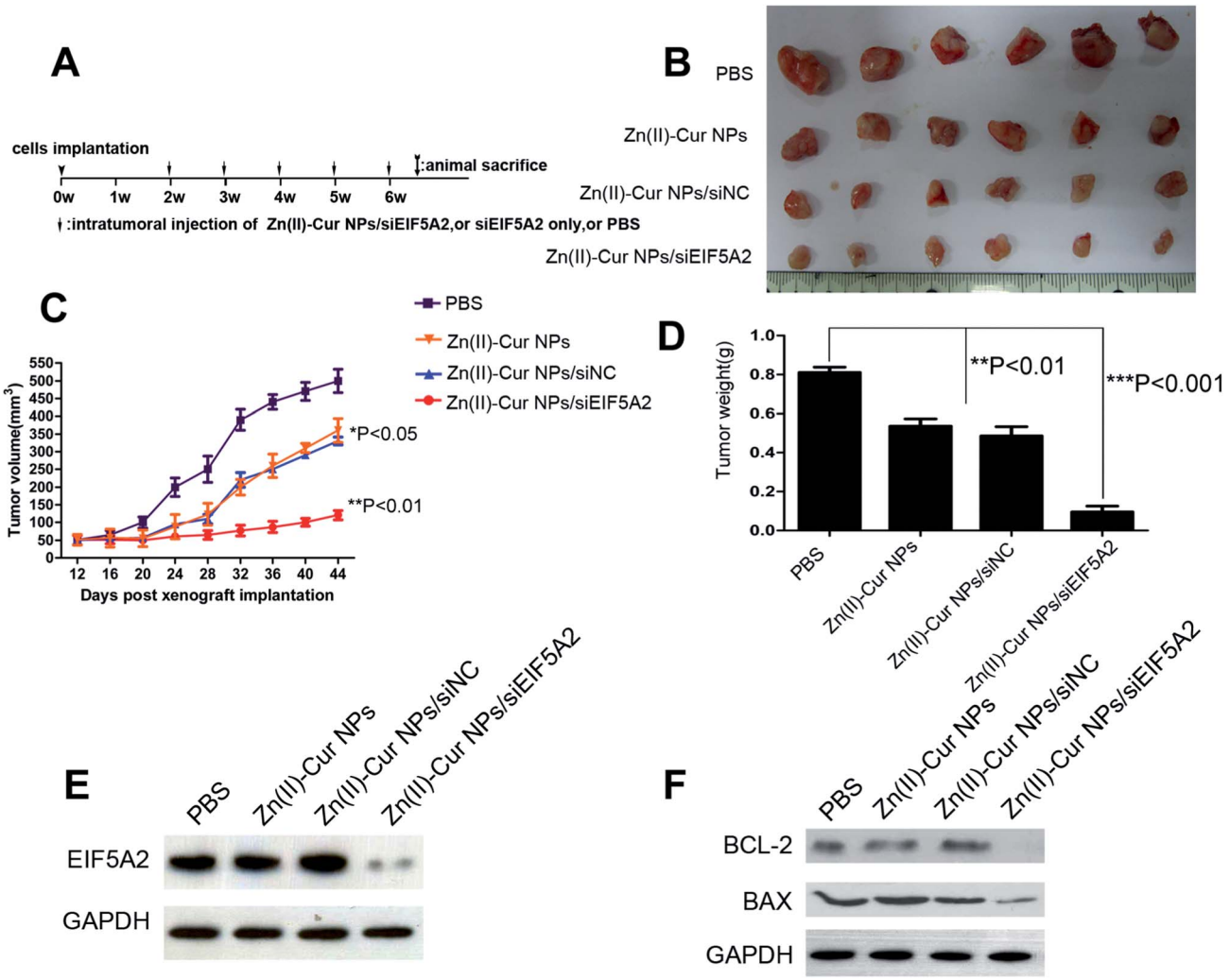

Fig. 9 (A) The timeline for the assessment of *in vivo* antitumor activities of the Zn(II)–Cur NP/siEIF5A2 complex in a subcutaneous xenograft model. (B) Actual sizes of representative tumors are shown. (C) Zn(II)–Cur NPs/siEIF5A2 (20 μg of siEIF5A2 per injection, 50 : 1 mass ratio) was injected locally into the tumors when the tumors had reached about 100 mm^3 in volume at the end of 2 weeks. Tumor diameters were recorded using calipers and the tumor volume was investigated every four days using the formula volume $= W^2 \times L/2$. Results are presented as mean ± SD ($n = 6$ tumors). (D) Mean tumor weights (±SD) measured after mice were sacrificed ($n = 6$, $^*P < 0.05$, $^{**}P < 0.01$, and $^{***}P < 0.001$ compared to other groups). (E) Western blotting analysis of the tissue lysates was performed using anti-EIF5A2 and anti-GAPDH antibodies. (F) Western blotting analysis of the tissue lysates was performed using anti-BCL-2, anti-BAX, and anti-GAPDH antibodies.

animals were sacrificed. Consistent with the change of EIF5A2 protein, mice receiving Zn(II)–Cur NPs/siEIF5A2 clearly display a lower level of EIF5A2 protein expression in tumor tissue than mice receiving either Zn(II)–Cur NPs or Zn(II)–Cur NPs/siNC (Fig. 9E). Strong inhibition of expression of BCL-2 is also observed under the treatment of Zn(II)–Cur NPs/siEIF5A2, which is probably induced by the synergistic effects of curcumin and siEIF5A2. The ratio of BAX to BCL-2 also increases by injection of Zn(II)–Cur NPs or Zn(II)–Cur NPs/siNC due to the chemotherapy effect of curcumin.[8] However, there is no such significant change in BCL-2 protein levels but evident up-regulation of the protein expression of BAX after treatments with either unloaded Zn(II)–Cur NPs or Zn(II)–Cur NPs/siNC when compared to the PBS control (Fig. 9F). *In vivo* experimental results suggest that Zn(II)–Cur NPs inhibit migration of HBC cells at a particular low dose and the BAX/BCL-2 signaling pathway might be the downstream signal pathway of EIF5A2 in regulating bladder cancer proliferation and progression. To evaluate the side-effect of Zn(II)–Cur NPs, the experiments for time-dependent body weight were performed. As shown in Fig. S7† after 18 days' observations, no significant change in body weight was found for different groups.

Conclusions

The present study has demonstrated that tumor growth of human bladder cancer cells can be effectively suppressed when EIF5A2 siRNA and curcumin were simultaneously administrated using pH sensitive Zn(II)–curcumin complex nanospheres as carriers. The Zn(II)–curcumin nanoparticles are cheap and simple to prepare with high reproducibility, and have good biocompatibility and high cellular uptake. The positively

charged Zn(II)–Cur NPs can efficiently deliver siRNA into human bladder cancer cells, protect siRNA against enzymatic degradation, and facilitate the escape of loaded siRNA from the endosomes into the cytoplasm, which successfully down-regulates the targeted EIF5A2 oncogene and consequently inhibits cancer cell growth *in vitro* and *in vivo*. Complexation of Zn^{2+} with curcumin increases the aqueous solubility of poorly water-soluble curcumin for high cellular uptake and bioavailability. The Zn(II)–curcumin drug NPs can respond to intracellular acidic pH environments of tumor to increase the ratio of BAX to BCL-2, promoting acid-triggered intracellular drug release. Furthermore, Zn(II)–Cur NPs carrying siEIF5A2 exhibit good penetrability and protect siRNA from degradation in tumor tissues. Intratumoral injection of the Zn(II)–Cur NP/siEIF5A2 complex inhibits human bladder tumor growth in the xenograft murine model. *In vitro* and *in vivo* experiments have revealed that synergetic combination of chemotherapy and gene therapy of bifunctional Zn(II)–Cur NPs/siEIF5A2 results in higher therapeutic efficacy than the individual therapeutic protocols. All of these results suggest that the pH-sensitive Zn(II)–Cur NPs may serve as novel, safe and effective siRNA delivery carriers for combination therapy. In principle, our strategy can be extended to produce other multifunctional nanocarriers made from antitumor drug itself for realizing synergetic therapy effects such as chemo/gene therapeutics with high efficacy.

Acknowledgements

This work was supported by the National Basic Research Program of China (2010CB934700, 2011CB933700). The National Natural Science Foundation of China (21271165, 81372821, 81372357, 81172429) is gratefully acknowledged for their support.

Notes and references

1 (*a*) S.-M. Lee, T. V. O'Halloran and S. T. Nguyen, *J. Am. Chem. Soc.*, 2010, **132**, 17130–17138; (*b*) H. J. Mauceri, N. N. Hanna, M. A. Beckett, D. H. Gorski, M.-J. Staba, K. A. Stellato, K. Bigelow, R. Heimann, S. Gately, M. Dhanabal, G. A. Soff, V. P. Sukhatme, D. W. Kufe and R. R. Weichselbaum, *Nature*, 1998, **394**, 287–291; (*c*) H. Meng, W. X. Mai, H. Y. Zhang, M. Xue, T. Xia, S. J. Lin, X. Wang, Y. Zhao, Z. X. Ji, J. I. Zink and A. E. Nel, *ACS Nano*, 2013, **7**, 994–1005; (*d*) M. E. Muroski, J. M. Kogot and G. F. Strouse, *J. Am. Chem. Soc.*, 2012, **134**, 19722–19730; (*e*) B. Rubinfeld, A. Upadhyay, S. L. Clark, S. E. Fong, V. Smith, H. Koeppen, S. Ross and P. Polakis, *Nat. Biotechnol.*, 2006, **24**, 205–209; (*f*) S. Sengupta, D. Eavarone, I. Capila, G. Zhao, N. Watson, T. Kiziltepe and R. Sasisekharan, *Nature*, 2005, **436**, 568–572; (*g*) Y. Zhao, B. G. Trewyn, I. I. Slowing and V. S. Y. Lin, *J. Am. Chem. Soc.*, 2009, **131**, 8398–8400; (*h*) M. V. Yezhelyev, L. Qi, R. M. O'Regan, S. Nie and X. Gao, *J. Am. Chem. Soc.*, 2008, **130**, 9006–9012.

2 (*a*) M. Aouadi, G. J. Tesz, S. M. Nicoloro, M. Wang, M. Chouinard, E. Soto, G. R. Ostroff and M. P. Czech, *Nature*, 2009, **458**, 1180–1184; (*b*) J. C. Burnett and J. J. Rossi, *Chem. Biol.*, 2012, **19**, 60–71; (*c*) B. L. Davidson and P. B. McCray, *Nat. Rev. Genet.*, 2011, **12**, 329–340; (*d*) J. H. Jeong, S. H. Kim, M. Lee, W. J. Kim, T. G. Park, K. S. Ko and S. W. Kim, *J. Controlled Release*, 2010, **143**, 88–94; (*e*) T. S. Zimmermann, A. C. H. Lee, A. Akinc, B. Bramlage, D. Bumcrot, M. N. Fedoruk, J. Harborth, J. A. Heyes, L. B. Jeffs, M. John, A. D. Judge, K. Lam, K. McClintock, L. V. Nechev, L. R. Palmer, T. Racie, I. Röhl, S. Seiffert, S. Shanmugam, V. Sood, J. Soutschek, I. Toudjarska, A. J. Wheat, E. Yaworski, W. Zedalis, V. Koteliansky, M. Manoharan, H.-P. Vornlocher and I. MacLachlan, *Nature*, 2006, **441**, 111–114.

3 (*a*) D. Putnam, *Nat. Mater.*, 2006, **5**, 439–451; (*b*) T. M. Sun, J. Z. Du, Y. D. Yao, C. Q. Mao, S. Dou, S. Y. Huang, P. Z. Zhang, K. W. Leong, E. W. Song and J. Wang, *ACS Nano*, 2011, **5**, 1483–1494.

4 N. Juliane and F. C. Szoka, *Acc. Chem. Res.*, 2012, **45**, 1153–1162.

5 D. Luo and W. M. Saltzman, *Nat. Biotechnol.*, 2000, **18**, 33–37.

6 (*a*) S. C. Gupta, S. Prasad, J. H. Kim, S. Patchva, L. J. Webb, I. K. Priyadarsini and B. B. Aggarwal, *Nat. Prod. Rep.*, 2011, **28**, 1937–1955; (*b*) K. Singletary, C. MacDonald, M. Iovinelli, C. Fisher and M. Wallig, *Carcinogenesis*, 1998, **19**, 1039–1043.

7 P. Sanphui, N. R. Goud, U. B. R. Khandavilli, S. Bhanoth and A. Nangia, *Chem. Commun.*, 2011, **47**, 5013–5015.

8 J. I. Hong, M. Bose, J. Y. Ju, J. H. Ryu, X. X. Chen, S. M. Sang, M. J. Lee and C. S. Yang, *Carcinogenesis*, 2004, **25**, 1671–1679.

9 T. L. Chiu and C. C. Su, *Int. J. Mol. Med.*, 2009, **23**, 469–475.

10 (*a*) C. J. H. Porter, N. L. Trevaskis and W. N. Charman, *Nat. Rev. Drug. Discovery*, 2007, **6**, 231–248; (*b*) S. Wan, Y. Sun, X. Qi and F. Tan, *AAPS PharmSciTech*, 2012, **13**, 159–166; (*c*) Y. Cheng and T. Xu, *Eur. J. Med. Chem.*, 2005, **40**, 1188–1192.

11 X. Z. Zhao, T. Jiang, L. Wang, H. Yang, S. Zhang and P. Zhou, *J. Mol. Struct.*, 2010, **984**, 316–325.

12 M. Thomas and A. M. Klibanov, *Proc. Natl. Acad. Sci. U. S. A.*, 2003, **100**, 9138–9143.

13 Z. Liu, M. Winters, M. Holodniy and H. Dai, *Angew. Chem., Int. Ed.*, 2007, **46**, 2023–2027.

14 D. R. Radu, C.-Y. Lai, K. Jeftinija, E. W. Rowe, S. Jeftinija and V. S. Y. Lin, *J. Am. Chem. Soc.*, 2004, **126**, 13216–13217.

15 K. A. Woodrow, Y. Cu, C. J. Booth, J. K. Saucier-Sawyer, M. J. Wood and W. M. Saltzman, *Nat. Mater.*, 2009, **8**, 526–533.

16 W. Chen, J.-H. Luo, W.-F. Hua, F.-J. Zhou, M. C. Lin, H.-F. Kung, Y.-X. Zeng, X.-Y. Guan and D. Xie, *Cancer Epidemiol., Biomarkers Prev.*, 2009, **18**, 400–408.

17 N. Sanoj Rejinold, M. Muthunarayanan, V. Divyarani, P. Sreerekha, K. Chennazhi, S. Nair, H. Tamura and R. Jayakumar, *J. Colloid Interface Sci.*, 2011, **360**, 39–51.

18 (*a*) T.-Y. Cheang, S.-M. Wang, Z.-J. Hu, Z.-H. Xing, G.-Q. Chang, C. Yao, Y. Liu, H. Zhang and A.-W. Xu, *J. Mater. Chem.*, 2010, **20**, 8050–8055; (*b*) J. Wei, T. Cheang, B. Tang, H. Xia, Z. Xing, Z. Chen, Y. Fang, W. Chen, A. Xu, S. Wang and J. Luo, *Biomaterials*, 2013, **34**, 1246–1254.

19 D. T. Limmer, A. P. Willard, P. Madden and D. Chandler, *Proc.Natl. Acad. Sci. U. S. A.*, 2013, **110**, 4200–4205.
20 T. M. Kolev, E. A. Velcheva, B. A. Stamboliyska and M. Spiteller, *Int. J. Quantum Chem.*, 2005, **102**, 1069–1079.
21 K. i. Kiyomiya, S. Matsuo and M. Kurebe, *Life Sci.*, 1998, **62**, 1853–1860.
22 (*a*) J.-Z. Du, X.-J. Du, C.-Q. Mao and J. Wang, *J. Am. Chem. Soc.*, 2011, **133**, 17560–17563; (*b*) X.-Z. Yang, J.-Z. Du, S. Dou, C.-Q. Mao, H.-Y. Long and J. Wang, *ACS Nano*, 2011, **6**, 771–781.
23 Y. Zhang, C. Wang, C. Xu, C. Yang, Z. Zhang, H. Yan and K. Liu, *Chem. Commun.*, 2013, **49**, 7286–7288.
24 S. Asayama, S. Nishinohara and H. Kawakami, *Metallomics*, 2011, **3**, 680–682.
25 J.-M. Li, M.-X. Zhao, H. Su, Y.-Y. Wang, C.-P. Tan, L.-N. Ji and Z.-W. Mao, *Biomaterials*, 2011, **32**, 7978–7987.
26 S. T. Tharakan, T. Inamoto, B. Sung, B. B. Aggarwal and A. M. Kamat, *Biochem. Pharmacol.*, 2010, **79**, 218–228.